

Article

# Selective Adsorption-Based Separation of Flue Gas and Natural Gas in Zirconium Metal-Organic Frameworks Nanocrystals

Pengli Li <sup>1</sup>, Yongli Shen <sup>1</sup>, Dandan Wang <sup>1</sup>, Yanli Chen <sup>2,\*</sup> and Yunfeng Zhao <sup>1,\*</sup>

<sup>1</sup> Tianjin Key Laboratory of Advanced Functional Porous Materials, Institute for New Energy Materials & Low-Carbon Technologies, Tianjin University of Technology, Tianjin 300384, China; lp1929@163.com (P.L.); panger\_shen@126.com (Y.S.); 15510906816@163.com (D.W.)

<sup>2</sup> School of Materials Science and Engineering, Tianjin University of Technology, Tianjin 300384, China

\* Correspondence: yanlichen@live.com (Y.C.); yfzhao@tjut.edu.cn (Y.Z.); Tel.: +86-22-6021-6415 (Y.Z.)

Academic Editor: Takeji Takahiro

Received: 6 May 2019; Accepted: 8 May 2019; Published: 11 May 2019



**Abstract:** Carbon capture from flue gas and natural gas offers a green path to construct a net-zero emissions economic system. Selective adsorption-based gas separation by employing metal-organic frameworks (MOFs) is regarded as a promising technology due to the advantages of simple processing, easy regeneration and high efficiency. We synthesized two Zirconium MOFs (UiO-66 and UiO-66-NH<sub>2</sub>) nanocrystals for selective capture and further removal of CO<sub>2</sub> from flue gas and natural gas. In particular, UiO-66-NH<sub>2</sub> nanocrystals have a smaller grain size, a large amount of defects, and pending -NH<sub>2</sub> groups inside their pores which display effective CO<sub>2</sub> selective adsorption abilities over CH<sub>4</sub> and N<sub>2</sub> with the theoretical separation factors of 20 and 7. This breakthrough experiment further verified the selective adsorption-based separation process of natural gas and flue gas. In one further step, we used the Monte Carlo simulation to investigate the optimized adsorption sites and energy of CO<sub>2</sub>, N<sub>2</sub> and CH<sub>4</sub> molecules in the gas mixture. The significantly large adsorption energy of CO<sub>2</sub> (0.32 eV) over N<sub>2</sub> (0.19 eV) and N<sub>2</sub> (0.2 eV) may help us to reveal the selective adsorption mechanism.

**Keywords:** UiO-66; carbon capture; gas separation; flue gas; methane

## 1. Introduction

Carbon dioxide (CO<sub>2</sub>) is regarded as the primary anthropogenic culprit for global warming and climate change, which is produced by fossil fuel [1]. The atmospheric CO<sub>2</sub> concentration has increased approximately 300–400 ppm over the last 50 years (1960–2016) [2], and is speculated to reach more than 500 ppm by 2050 [3]. The main emission source of CO<sub>2</sub> is the combustion of fossil fuels such as coal, oil, and natural gas. Carbon capture is broadly identified as possessing the great potential to play a critical role in meeting climate change targets [4]. Effective carbon capture is regarded as one key node of the net-zero emission energy system [1]. The major demand for carbon capture comes from the treatment of CO<sub>2</sub> mixture gas including power-plant flue gas, raw natural gas, coal-bed gas, and biogas in which CO<sub>2</sub> is in wide concentration range and is mixed with different gases. For example, about 5%–15% of CO<sub>2</sub> is majorly mixed with N<sub>2</sub> in power-plant flue gas, and a wide range of CO<sub>2</sub> is regarded as an impurity of methane (CH<sub>4</sub>) for the raw natural gas (CH<sub>4</sub>: >90%, CO<sub>2</sub>: 0.5–1%) and coal-bed (CH<sub>4</sub>: >50%, N<sub>2</sub>: ~40%, CO<sub>2</sub>: ~1%) [5] gas as well as biogas (CH<sub>4</sub>: ~50%, CO<sub>2</sub>: ~50%) [6]. Therefore, how to selectively capture CO<sub>2</sub> in a wide range of gas components is a big challenge and is considered as one of seven major challenges in the field of separation processes within chemical engineering [7].

Various CO<sub>2</sub> capture technologies, including absorption, adsorption, cryogenics, and membranes, have been developed [8,9]. Currently, the benchmark industrially demonstrated process for

post-combustion CO<sub>2</sub> capture technology from power plants is amines solvent-based absorption. However, high energy is required in the regeneration process and the corrosive and volatile nature of the amines also presents problems [10,11]. Physisorption of CO<sub>2</sub> into microporous materials has been widely studied in recent years. The heat of adsorption of CO<sub>2</sub> onto porous sorbents is normally less than 50 kJ mol<sup>-1</sup> which is much smaller than chemisorption, and thus, the regeneration process has low-energy consumption and is environment-friendly [12,13]. A variety of microporous adsorbents including zeolite, activated carbons, metal-organic frameworks (MOFs) [14], and covalent-organic frameworks (COFs) [15,16] have been developed. Among these porous materials, MOFs have attracted significant attention owing to their enormous variety of interesting structural topologies and wide range of potential applications. These are constructed from metal ions as nodes and multidentate organic ligands as linkers. Adsorption and further separation of CO<sub>2</sub> in MOFs have been intensely studied [12,17–19], and a variety of strategies of metal open-site, amino-functionalization, and pore size optimization have been successfully demonstrated. However, the major drawbacks of stabilities and robust fabrication limited the further application of MOFs. UiO-66 is a metal-organic skeleton material containing Zr developed by the University of Oslo in Norway in 2008 [20]. UiO-66 and its –NH<sub>2</sub> modified derivatives are considered good adsorbents for molecule and ion adsorption in gas [21] and solution [22,23] due to their excellent stability in heat and water [24]. In particular, UiO-66-NH<sub>2</sub>, which contains amine pendant groups on benzene dicarboxylate linkers, has showed the potential for selective adsorption of CO<sub>2</sub> over N<sub>2</sub> or CH<sub>4</sub> when simply comparing the gas adsorption performance under conditions of equilibrium [25–27]. UiO-66-NH<sub>2</sub> nanocrystals were also used as filler to prepare a mixed-matrix membrane for CO<sub>2</sub>/N<sub>2</sub> [28] and CO<sub>2</sub>/CH<sub>4</sub> [29] separation. However, the carbon capture from the mixture gas is a non-equilibrium process; the dynamic research of CO<sub>2</sub>, CH<sub>4</sub> and N<sub>2</sub> selective adsorption and separation at both the experimental and the theoretical level requires more attention, which is critical to develop sustainable carbon capture technology.

In this work, we synthesized UiO-66 and UiO-66-NH<sub>2</sub> nanocrystals in a fast and easy way. UiO-66 and UiO-66-NH<sub>2</sub> displayed CO<sub>2</sub> selective adsorption ability over N<sub>2</sub> and CH<sub>4</sub>. The ideal selectivity of CO<sub>2</sub>/N<sub>2</sub> and CO<sub>2</sub>/CH<sub>4</sub> in UiO-66-NH<sub>2</sub> was calculated to be 20 and 7 under 298K, respectively. The carbon capture from flue gas and raw natural gas was performed in a UiO-66-NH<sub>2</sub> packed column by breakthrough experiments. CO<sub>2</sub> molecules can be effectively removed with the selective factor of seven (CO<sub>2</sub>/N<sub>2</sub>, 15/85 in volume) and two (CO<sub>2</sub>/CH<sub>4</sub>, 10/90 in volume), respectively. In addition, the separation process was further simulated by theoretical calculation to recover the binding energies of gas molecules and prefer gas adsorption abilities of UiO-66-NH<sub>2</sub>.

## 2. Results

### 2.1. Synthesis and Characterization

UiO-66 and UiO-66-NH<sub>2</sub> were synthesized in a convenient process, in which the nanocrystals were prepared in a short time (total 2.5 h) under ambient pressure without using pressure autoclave. Typically, Zirconium tetrachloride (ZrCl<sub>4</sub>), hydrochloric acid (HCl, 37 wt%), terephthalic acid, and *N,N*-Dimethylformamide (DMF) were placed in a glass vial (100 mL) and vigorously stirred for 30 min at 80 °C. After centrifugation, washing, and drying, UiO-66 and UiO-66-NH<sub>2</sub> particles were then obtained.

The morphologies of UiO-66 and UiO-66-NH<sub>2</sub> crystals were firstly characterized through scanning electron microscopy (SEM) and transmission electron microscopy (TEM). Figure 1a shows the morphology of UiO-66, where the typical particle size in the range of 100–200 nm was found. Synthesized UiO-66-NH<sub>2</sub> possessed a smaller particle size with the typical size less than 100 nm (Figure 1b). Furthermore, the TEM images also showed that the UiO-66 (Figure 1c) and UiO-66-NH<sub>2</sub> (Figure 1d) particles possess an irregular shape with the mean particle size around 200 nm (UiO-66) and approximate 100 nm (UiO-66-NH<sub>2</sub>), respectively, and this was mutually verified by SEM results. The energy-dispersive X-ray spectroscopy (EDS) mapping was employed to investigate the elements'

distribution. As indicated in Figure 1e,f, the elements Zr and O uniformly spread over the particles, while the element N was also founded from UiO-66-NH<sub>2</sub> which is derived from the -NH<sub>2</sub> group of the ligand (2-aminoterephthalic acid).

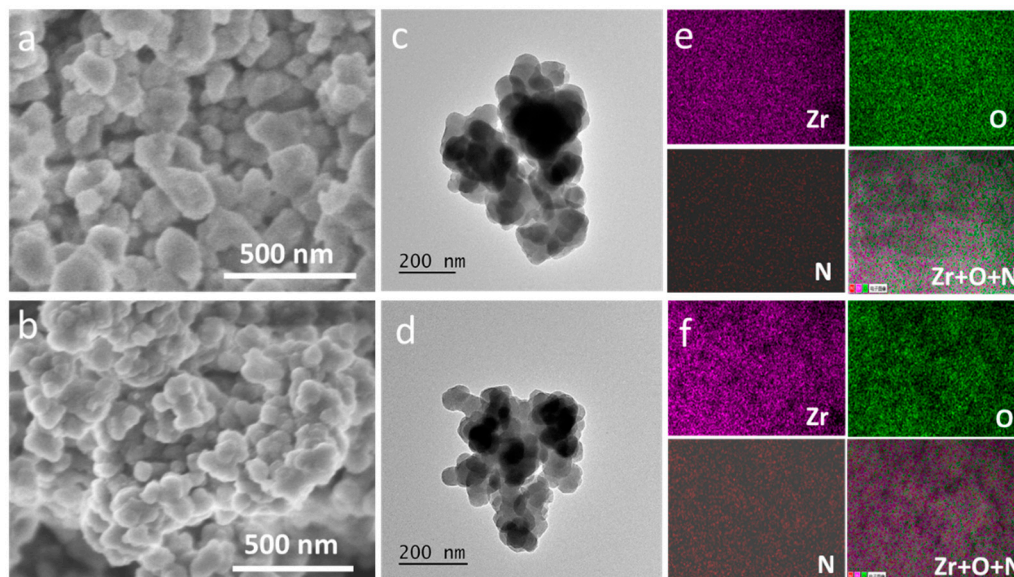


**Figure 1.** The SEM (a), TEM (c) and EDS (e) mapping images of UiO-66; the SEM (b), TEM (d) and EDS (f) mapping images of UiO-66-NH<sub>2</sub>.

The crystal phase was then examined by X-ray powder diffraction (XRD). Figure 2a shows the major diffraction patterns of UiO-66 and UiO-66-NH<sub>2</sub>, where the peaks were well consistent with the simulated pattern of UiO-66 reported previously [20]. However, the as-synthesized UiO-66 and UiO-66-NH<sub>2</sub> particles exhibited broad peaks with low intensity, suggesting that some disorder and therefore large number of defects would exist in UiO-66 and UiO-66-NH<sub>2</sub> [30,31]. Recent studies have shown that defects in MOFs provide a positive influence on catalysis, adsorption, and proton conductivity [32]. Fourier-transform infrared spectroscopy (FTIR) spectra in Figure 2b shows the chemical information of UiO-66 and UiO-66-NH<sub>2</sub>. They have similar vibrational peaks in the FTIR spectra. The characteristic peak around 3403 cm<sup>-1</sup> was ascribed to the vibrational mode of the O-H group, which was related to the adsorbed water from the surface of the samples. A lot of intense peaks in the range of 1700–1200 cm<sup>-1</sup> were derived from asymmetrical and symmetrical stretching vibrations of the carboxylate groups. The peaks at 800–600 cm<sup>-1</sup> might be ascribed to a Zr-O bond. Especially, the peaks of 1390 and 1264 cm<sup>-1</sup> were attributed to the vibrational mode of the C-N band in FTIR spectra of UiO-66-NH<sub>2</sub>, which originate from the -NH<sub>2</sub> group of ligands of UiO-66-NH<sub>2</sub>. We use acid-base titration to further determine the existence and quantity of defects in UiO-66 and UiO-66-NH<sub>2</sub>. The titration curves for UiO-66 and UiO-66-NH<sub>2</sub> are shown in Figure 2c. There is a slow break in the curve between the pH of five and seven. To better visualize the various equivalence points, the first derivative of the titration curve is further plotted. The results show the distinct equivalence points corresponding to the pK<sub>a</sub> values in Table 1. These defects can be assigned to bridging-OH, acetic acid, and Zr-OH<sub>2</sub>, respectively [31]. The thermal stability was also investigated by thermal gravimetric analysis (TGA) (Figure 2d), the weight loss before 100 °C was due to the removal of adsorbed small molecules from air, ca. CO<sub>2</sub> and H<sub>2</sub>O. No obvious decomposition was found before 500 °C for UiO-66 and 300 °C for UiO-66-NH<sub>2</sub> indicating their superior stability [20].

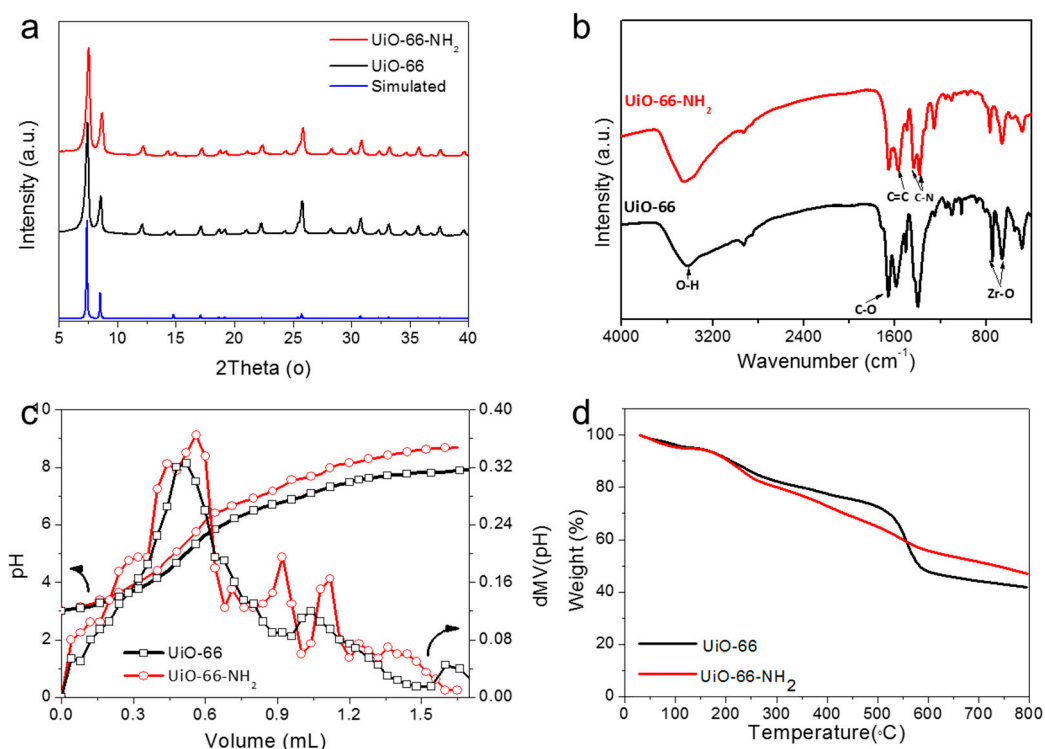


**Figure 2.** X-ray diffraction patterns (a), FTIR spectra (b), acid-base titration curves (c), and TGA (d) curves of UiO-66 and UiO-66-NH<sub>2</sub>.

**Table 1.** Calculated pKa's and corresponding equivalence volumes for UiO-66 and UiO-66-NH<sub>2</sub> samples that were analyzed by acid-base titration.

MOFs	Bridging-OH		Acetate		Zr-OH <sub>2</sub>	
	pKa	Equi. vol. (mL)	pKa	Equi. vol. (mL)	pKa	Equi. vol. (mL)
UiO-66	3.47	0.52	5.04	1.04	6.47	1.60
UiO-66-NH <sub>2</sub>	3.82	0.56	4.92	0.92	5.76	1.12

## 2.2. Pore Structure and Gas Selective Adsorption

The textural characteristics (surface areas, pore size and pore volume) of UiO-66 and UiO-66-NH<sub>2</sub> nanocrystals are evaluated by N<sub>2</sub> adsorption and desorption analysis at 77 K. The nitrogen adsorption-desorption isotherms and the pore size distribution of UiO-66 and UiO-66-NH<sub>2</sub> are shown in Figure 3. The characteristic of isotherms was in accord with type-II adsorption isotherms where the primary adsorption occurred at low relative pressures <0.1 indicated the formation of a highly microporous material with the possibility of a narrow pore size distribution of UiO-66 and UiO-66-NH<sub>2</sub>. The adsorption curve climbed rapidly at P/P<sub>0</sub> values greater than 0.95 indicating the capillary condensation derived from the aggregation of nanoparticles or defects. The results showed that UiO-66 and UiO-66-NH<sub>2</sub> had a large Brunauer–Emmett–Teller (BET) surface area of 1308 and 1104 m<sup>2</sup> g<sup>-1</sup>, respectively, and it was in good agreement with previously reported UiO-66 structures that contain defects [31,33]. The pore distributions of UiO-66 and UiO-66-NH<sub>2</sub> were further investigated through the Nonlocal Density Functional Theory (NLDF) method based on the adsorption data. The bimodal pore distributions of ultramicropores (<0.7 nm) and supermicropores (0.7–2 nm) were probed as displayed in Figure 3b. Moreover, the pore volume was 0.533 (UiO-66) and 0.462 (UiO-66-NH<sub>2</sub>) cm<sup>3</sup> g<sup>-1</sup>, respectively. These results demonstrated that the prepared UiO-66 and UiO-66-NH<sub>2</sub> possess a high surface area in the micropore range and thus enabled a desirable adsorption capability.

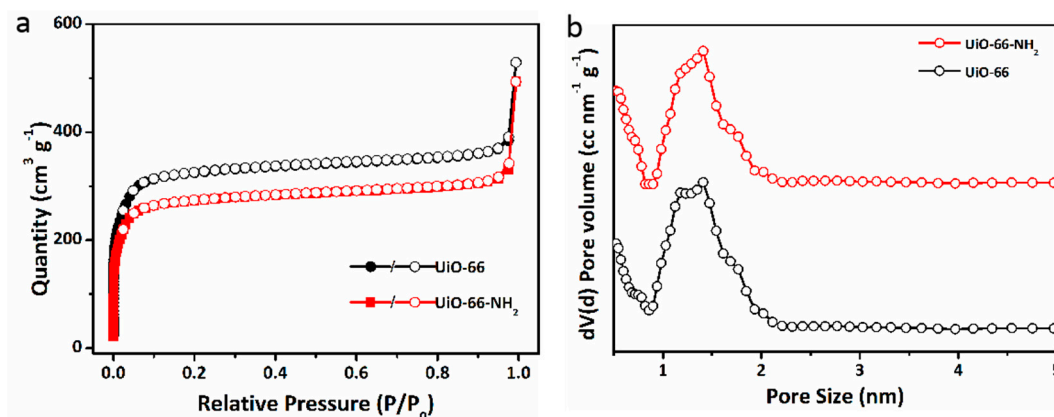


**Figure 3.**  $N_2$  isotherms at 77 K (a) and pore distribution curves (b) calculated from absorption curves by the NLDFT mode of UiO-66 and UiO-66-NH<sub>2</sub>.

With their combination of nanosized, abundant defects and a large number of micropores, UiO-66 and UiO-66-NH<sub>2</sub> demonstrated that they have great potential in the field of gas adsorption and separation. The CO<sub>2</sub>, CH<sub>4</sub> and N<sub>2</sub> adsorption-desorption curves are given in Figure 4, where the isotherms are recorded under the two temperatures of 273K and 298K, respectively. UiO-66 and UiO-66-NH<sub>2</sub> exhibited excellent adsorption performance for CO<sub>2</sub> at different temperatures. As shown in Figure 4, the CO<sub>2</sub>, CH<sub>4</sub> and N<sub>2</sub> equilibrium adsorption capacities of UiO-66 were 61 cm<sup>3</sup> g<sup>-1</sup>, 13.6 cm<sup>3</sup> g<sup>-1</sup>, and 2.7 cm<sup>3</sup> g<sup>-1</sup> at 273 K and 100 kPa, respectively. For 298 K and 100 kPa, the uptake capacities of CO<sub>2</sub>, CH<sub>4</sub>, and N<sub>2</sub> were 33.4 cm<sup>3</sup> g<sup>-1</sup>, 8.1 cm<sup>3</sup> g<sup>-1</sup>, and 3.1 cm<sup>3</sup> g<sup>-1</sup>, respectively. The enhancement gas adsorption abilities were found from UiO-66-NH<sub>2</sub>. The CO<sub>2</sub>, CH<sub>4</sub>, and N<sub>2</sub> equilibrium adsorption capacity of UiO-66-NH<sub>2</sub> were 68 cm<sup>3</sup> g<sup>-1</sup>, 13.9 cm<sup>3</sup> g<sup>-1</sup>, and 2.8 cm<sup>3</sup> g<sup>-1</sup> at 273 K and 100 kPa, respectively. And they were 37.6, 8.1, and 2.9 cm<sup>3</sup> g<sup>-1</sup> at 298 K and 100 kPa. UiO-66-NH<sub>2</sub> and UiO-66 have moderate CO<sub>2</sub> uptakes which are comparable with MIL-100(Cr) (50) [34], UiO-66 (38) [27], MAC-4 (37.2) [35], IRMOF-1 (27.3) [36], and MOF-177 (19.8) [36] at atmosphere condition.

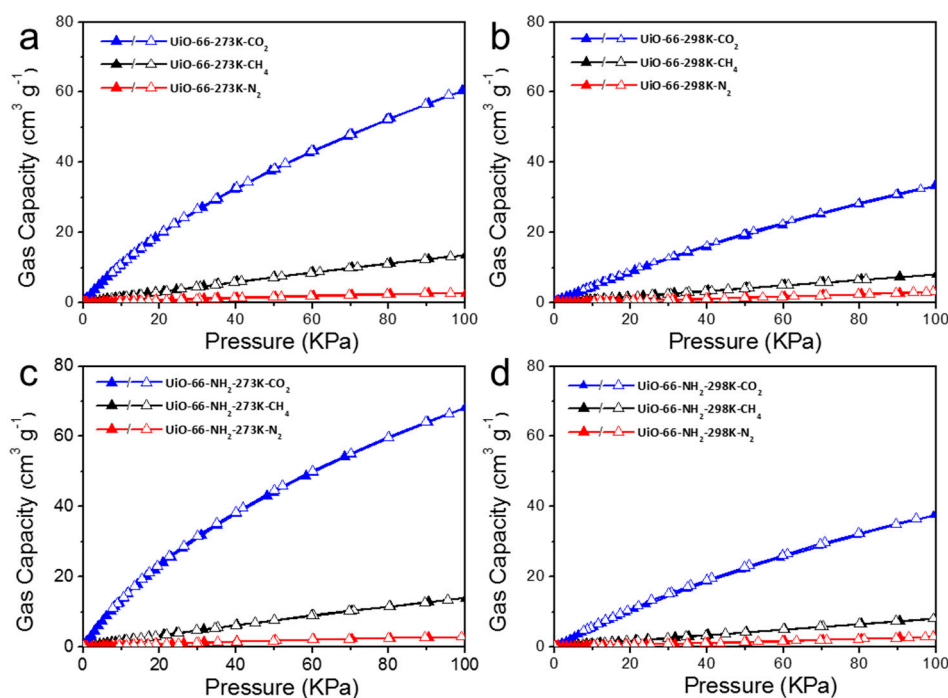


**Figure 4.** CO<sub>2</sub>, CH<sub>4</sub>, and N<sub>2</sub> adsorption-desorption isotherms of UiO-66 at 273K (a) and 298K (b); UiO-66-NH<sub>2</sub> at 273 K (c) and 298 K (d).

The CO<sub>2</sub> capacity was further normalized to the pore volume to recover the affection of chemical components of UiO-66 and UiO-66-NH<sub>2</sub>. As indicated in Figure 5, UiO-66-NH<sub>2</sub> has obvious larger normalized CO<sub>2</sub> adsorption values than UiO-66. This phenomenon showed that the –NH<sub>2</sub> group of ligands in UiO-66-NH<sub>2</sub> may contribute more to the CO<sub>2</sub> molecule adsorption sites, and this conclusion coincides with Ethiraj's conclusion [37]. More importantly, UiO-66 and UiO-66-NH<sub>2</sub> display apparent higher CO<sub>2</sub> adsorption capacity than CH<sub>4</sub> and N<sub>2</sub> under the same temperatures and pressures, meaning that it has potential to remove CO<sub>2</sub> from CH<sub>4</sub> and N<sub>2</sub> by selective adsorption.

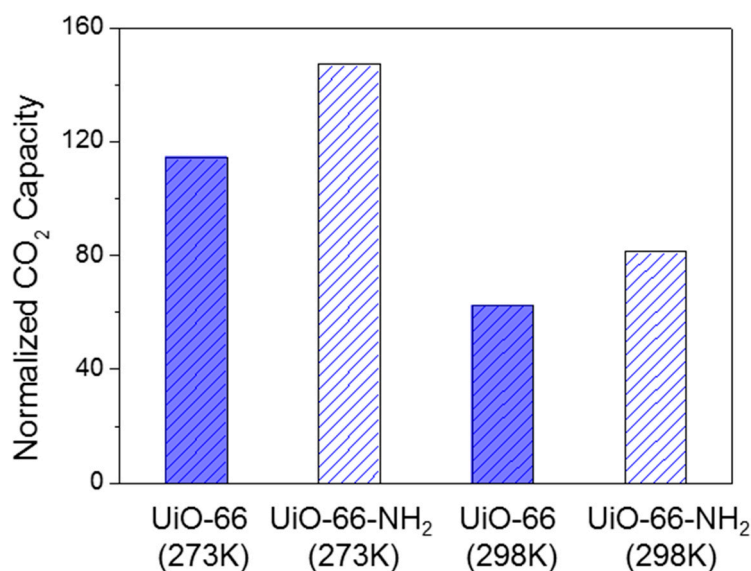


Figure 5. The normalized CO<sub>2</sub> capacities of UiO-66 and UiO-66-NH<sub>2</sub>.

### 2.3. Dynamic Separation of Flue Gas and Natural Gas

The gas selective separation abilities of UiO-66 and UiO-66-NH<sub>2</sub> were firstly evaluated through ideal adsorbed solution theory (IAST), which is widely used to estimate the potential of gas separation of porous materials based on single gas equilibrium adsorption curves [38]. Single-component isotherms of CO<sub>2</sub>/N<sub>2</sub> (15/85 in volume) and CO<sub>2</sub>/CH<sub>4</sub> (10/90 in volume) at 298 K were fitted, where the component was the typical composite of flue gas (CO<sub>2</sub> and N<sub>2</sub>) and raw natural gas (CO<sub>2</sub> and CH<sub>4</sub>). As shown in Figure 6, the adsorption selectivity of CO<sub>2</sub>/N<sub>2</sub> were calculated to be about 16 (UiO-66) and 20 (UiO-66-NH<sub>2</sub>) at a pressure of 100 kPa and 298 K, respectively, which is comparable with UiO-66 (17.8) [25] and MOF-505 (27.8) [39]. The CO<sub>2</sub>/CH<sub>4</sub> selectivity was about 6 (UiO-66) and 7 (UiO-66-NH<sub>2</sub>) at the same condition, respectively, which is at the same level with MIL-100(Cr) (8) [34], MOF-505 (7.6) [39], and MAF-66 (5.8) [40]. The IAST results indicated the feasibility of UiO-66-NH<sub>2</sub> for practical application in the separation of CO<sub>2</sub>/N<sub>2</sub> and CO<sub>2</sub>/CH<sub>4</sub>.

To evaluate the potential for real separation of the gas mixture of CO<sub>2</sub>/N<sub>2</sub> and CO<sub>2</sub>/CH<sub>4</sub> of UiO-66-NH<sub>2</sub>, the breakthrough experiments were carried out with binary mixtures of CO<sub>2</sub>/N<sub>2</sub> (15:85, *v/v*) and CO<sub>2</sub>/CH<sub>4</sub> (10:90, *v/v*) on a home-made column breakthrough setup (supporting information) which is the typical composition of flue gas and nature gas. As shown in Figure 6b, the results suggest the high-efficiency separation of N<sub>2</sub> from 15:85 CO<sub>2</sub>/N<sub>2</sub> by flowing the mixture gas over a packed column of UiO-66-NH<sub>2</sub>. It could be clearly observed that the N<sub>2</sub> first breakthrough was at 7 s, while the CO<sub>2</sub> could not be detected before its breakthrough point at 49 s. The separation factor was calculated to be seven following the calculation procedure provided in the supporting information. As shown in Figure 6d, the dynamic separation experiment of CO<sub>2</sub>/CH<sub>4</sub> mixed gas (10/90 in volume ration; flow speed of 2 mL min<sup>-1</sup>) was also examined under room temperature (298 K). The breakthrough curves can be divided into three segments based on their adsorption characteristics. The net breakthrough times (with the dead time deducted) of CO<sub>2</sub> and CH<sub>4</sub> were 114 and 226 s, respectively, giving a

$\text{CO}_2/\text{CH}_4$  (10/90) separation factor of about two. Therefore, the ability of selective adsorption and further remove  $\text{CO}_2$  from flue gas and natural gas of UiO-66- $\text{NH}_2$  has been demonstrated.

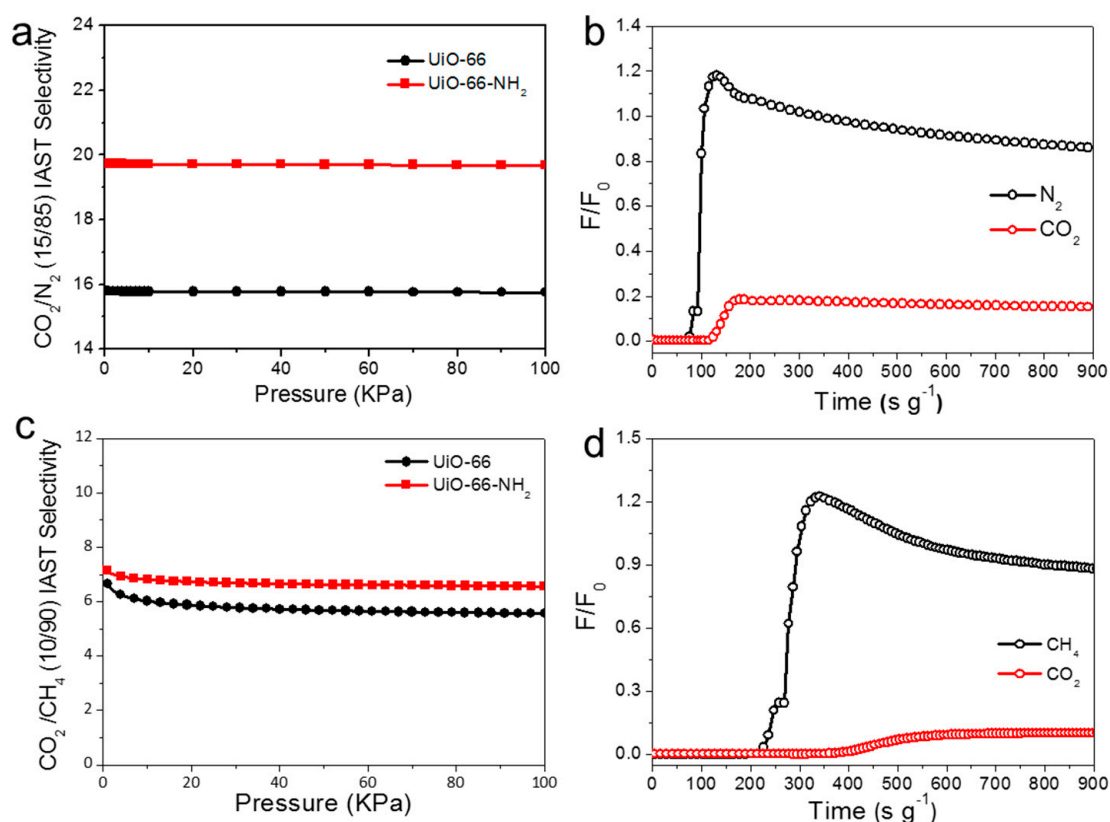


**Figure 6.** The IAST (a) and breakthrough separation curves (b) of  $\text{CO}_2/\text{CH}_4$  (10/90 in volume ratio) of UiO-66 and UiO-66- $\text{NH}_2$ ; the IAST (c) and breakthrough separation (d) curves (s) of  $\text{CO}_2/\text{N}_2$  (15/85 in volume ratio) of UiO-66 and UiO-66- $\text{NH}_2$ .

#### 2.4. Monte Carlo Simulation of Gas Selective Adsorption

A simple MC simulation was further carried out to analyze the distribution position and adsorption energy of  $\text{CO}_2$ ,  $\text{N}_2$  and  $\text{CH}_4$  in UiO-66- $\text{NH}_2$ . The simulation results showed that  $\text{CO}_2$ ,  $\text{N}_2$ , and  $\text{CH}_4$  molecules were mainly distributed in the cage surrounded by three ligands of UiO-66- $\text{NH}_2$  (Figure 7a). At the initial state, one  $\text{CO}_2$  molecule and seven  $\text{N}_2$  or  $\text{CH}_4$  molecules were placed in the cage to follow the chemical components of flue gas and raw natural gas, respectively. The optimized structures for  $\text{CO}_2$  and  $\text{N}_2$  or  $\text{CO}_2$  and  $\text{CH}_4$  are shown in Figure 7b,c, respectively. Small molecules were found to be located in the middle of the triangle area which implies that the weak interactions may rest between small molecules and UiO-66- $\text{NH}_2$ . To prove these weak intermolecular interactions, an Independent Gradient Model [41] was carried out for those two structures in Figure 7b,c. The scatter plots for the  $\delta$  function versus the  $\text{sign}(\lambda_2)\rho$  including intermolecular (red area) and intramolecular (black area) interactions were shown in Figure 7d,e, where the  $\text{sign}(\lambda_2)\rho$  is the sign of the second largest eigenvalue  $\lambda_2$  of the electron-density Hessian matrix multiplied by the electron density. It could be seen that the electron density of intermolecular interaction is not very large, but not very close to zero either. Based on this we can speculate that the intermolecular interactions in those two systems are weak interactions. The adsorption energy for  $\text{CO}_2$ ,  $\text{N}_2$ , and  $\text{CH}_4$  are estimated to be 0.32, 0.19, and 0.20 eV, respectively. It can be speculated that the  $\text{CO}_2$  and  $\text{CH}_4$  or  $\text{CO}_2$  and  $\text{N}_2$  mixed gases can be effectively separated by this MOF material, which is consistent with the experimental results.

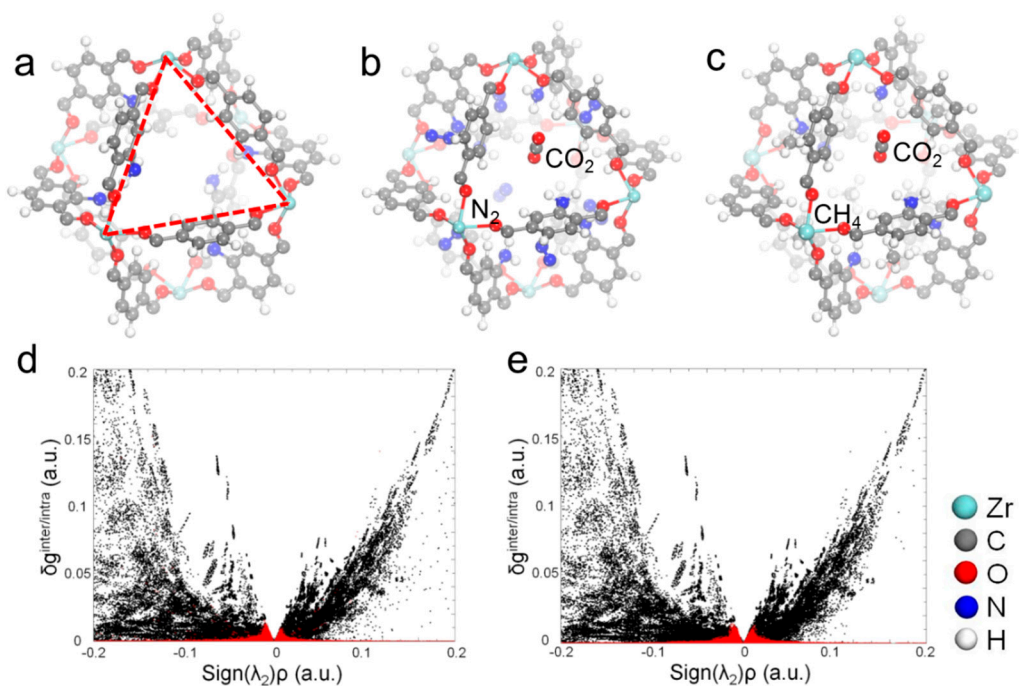


**Figure 7.** Optimized structures and intermolecular interactions between CO<sub>2</sub>, N<sub>2</sub> and CH<sub>4</sub>. Stable porous cage structure of UiO-66-NH<sub>2</sub> (a), stable adsorption structure for CO<sub>2</sub> and N<sub>2</sub> adsorption in UiO-66-NH<sub>2</sub> (b), stable adsorption structure for CO<sub>2</sub> and CH<sub>4</sub> adsorption in UiO-66-NH<sub>2</sub> (c), scatter plot for  $\delta$  function versus  $\text{sign}(\lambda_2)\rho$  of CO<sub>2</sub> and N<sub>2</sub> (d) and CO<sub>2</sub> and CH<sub>4</sub> (e) adsorption in UiO-66-NH<sub>2</sub>.

### 3. Materials and Methods

#### 3.1. Chemicals and Characterizations

The chemicals used were Zirconium chloride (ZrCl<sub>4</sub>,  $\geq 99.5\%$ ), terephthalic acid (99%), 2-aminoterephthalic acid (99%), hydrochloric acid (HCl, 5%), and *N,N*-Dimethylformamide (DMF). All chemicals were used as received without further purification. Powder X-ray diffraction patterns (XRD) were recorded on a Rigaku Ultima Iv X-ray diffractometer (Cu K $\alpha$ ,  $\lambda = 1.5406 \text{ \AA}$ , Rigaku, Tokyo, Japan,) at a scan rate of  $10^\circ \text{ min}^{-1}$  in the  $2\theta$  range from  $3^\circ$  to  $80^\circ$ . Fourier transform infrared spectroscopy (FTIR) spectra were measured using Frontier MidIR FTIR (PerkinElmer, Waltham, MA, USA) with the KBr pellet technique in the range  $400\text{--}4000 \text{ cm}^{-1}$ . The morphologies of the materials were observed using a Verios 460L scanning electron microscope (SEM, FEI, Hillsboro, OR, USA) and a Tecnai G2 Spirit TWIN transmission electron microscope (TEM, FEI, Hillsboro).

#### 3.2. Synthesis of UiO-66 and UiO-66-NH<sub>2</sub>

A total of 0.625 g of ZrCl<sub>4</sub> and 5 mL of 37% HCl aqueous solution were mixed and dissolved in 10 mL of DMF. After 30 min of ultrasonication, 0.615 g of terephthalic acid dissolved in 50 mL of DMF was added to the former solution of ZrCl<sub>4</sub> and HCl, and the whole solution was further sonicated by using a batch sonication (Kunshan Ultrasonic Instruments Co., Ltd., KQ-100, Kunshan, Jiangsu, China) with the output power of 100 W and the frequency of 40 kHz for the next 30 min. The solution was then kept in a 100 mL glass vial at  $80^\circ \text{C}$  statically without stirring or ultrasonication at  $80^\circ \text{C}$  for 2 h. UiO-66-NH<sub>2</sub> was prepared following the same process except that 2-aminoterephthalic acid was used to replace the terephthalic acid.

#### 3.3. Acid-Base Titrations

A total of 40 mg of sample (activated for 12 h at  $150^\circ \text{C}$ ) was added to a 100 mL beaker. An equivalent volume of a 0.01 M NaNO<sub>3</sub> solution was added and allowed to equilibrate for 18 h.

Preceding each titration, a stir bar was added to the beaker and the pH was adjusted to a value of 3.00 with 0.1 M HCl. Following this, the solution was titrated with 0.1 M NaOH of solution (adding 0.04 mL NaOH solution at a time and stirring evenly) with a pH value of 8.

### 3.4. Gas Adsorption Measurement

The N<sub>2</sub> sorption isotherms at 77 K and the gas adsorption isotherms of CO<sub>2</sub>, CH<sub>4</sub>, and N<sub>2</sub> at two different temperatures (273 and 298 K) were measured by using a Autosorb-iq3 surface area and porosimeter analyzer (Quantachrome, Boynton Beach, FL, USA). The temperatures (273 and 298 K) were controlled by means of a circulating bath. The samples were degassed at 473 K for 10 h under a vacuum of 10<sup>-5</sup> mmHg before the measurements. The pore size distributions and micropore surface areas were determined using the nonlocal density function theory (NLDFT) method. Gases with a high purity of over 99.995% were used.

### 3.5. Breakthrough Experiments

The breakthrough experiments of flue gas and natural gas separation were conducted in a home-made apparatus as illustrated in our previous reports [42,43].

The absolute adsorbed amount of gas *i* (*q<sub>i</sub>*) was calculated from the breakthrough curve by the equation:

$$q_i = \frac{F_i \times t_0 - V_{dead} - \int_0^{t_0} F_e \Delta t}{m}$$

where *F<sub>i</sub>* = influent flow rate of the specific gas (cm<sup>3</sup> min<sup>-1</sup>); *t<sub>0</sub>* = adsorption time (min); *V<sub>dead</sub>* = dead volume of the system (cm<sup>3</sup>); *F<sub>e</sub>* = effluent flow rate of the specific gas (cm<sup>3</sup> min<sup>-1</sup>); *m* = mass of the sorbent (g).

The selectivity of the breakthrough experiment is defined as  $\alpha = (q_1/y_1)/(q_2/y_2)$ , where *y<sub>i</sub>* is the mole fraction of gas *i* in the gas mixture.

### 3.6. DFT Calculations

Monte Carlo (MC) simulations are carried out with the adsorption locator module with the universal force field [44]. All the geometric optimization calculations were performed using the generalized gradient approximation (GGA) with the Perdew–Burke–Ernzerhof (PBE) functional [45] as implemented in the all-electron DMol<sup>3</sup> code [46,47]. The double numerical plus polarization (DNP) basis set was used throughout the calculations. The convergence criteria were set to be 2 × 10<sup>-5</sup> Ha, 0.004 Ha Å<sup>-1</sup>, and 0.005 Å for the energy, the force, and the displacement convergences, respectively. A self-consistent field (SCF) density convergence with a threshold value of 1 × 10<sup>-5</sup> Ha was specified. Independent Gradient Model analysis were carried out using Multiwfn software [48]. A complete MOF channel structure was cut-off from the single-crystal structure of UiO-66. All dangling bonds in the MOF structure (Zr atoms) were saturated by hydroxy groups.

## 4. Conclusions

In summary, we synthesized crystals of UiO-66 and UiO-66-NH<sub>2</sub> in nano-size with a high surface area and abundant defects. UiO-66 and UiO-66-NH<sub>2</sub> have selective gas adsorption ability of CO<sub>2</sub> over CH<sub>4</sub> and N<sub>2</sub>. The pure N<sub>2</sub> and CH<sub>4</sub> can be obtained from the simulated flue gas (CO<sub>2</sub>/N<sub>2</sub>, 15/85) and from raw natural gas (CO<sub>2</sub>/CH<sub>4</sub>, 10/90) by a breakthrough operation, respectively. Especially, the separation factors of seven (CO<sub>2</sub>/N<sub>2</sub>) and two (CO<sub>2</sub>/CH<sub>4</sub>) were calculated from UiO-66-NH<sub>2</sub> indicating the potential applications for green separation. The results of MC simulation showed that CO<sub>2</sub> displayed preferential adsorption energy over N<sub>2</sub> or CH<sub>4</sub> in the gas mixture through UiO-66-NH<sub>2</sub>. This dynamic study from theoretical and experimental aspects may provide an insight into the selective adsorption and separation of the gases.

**Author Contributions:** Y.Z. and Y.C. conceived and designed the experiments; P.L. fabricated the materials; P.L. and D.W. analyzed the data; Y.S. performed the theoretical calculation; Y.Z. and Y.C. wrote the manuscript.

**Funding:** This research was funded by National Natural Science Foundation of China, grant number [21506148, 5171101212], Natural Science Foundation of Tianjin City, grant number [15JCYBJC52700, 16JCYBJC17000, 16ZXCLGX00120], the Scientific Research Program of Tianjin Municipal Education Commission, grant number [2017KJ248].

**Acknowledgments:** Y.Z. acknowledges support from the “Talent Program” of Tianjin University of Technology, “Youth Thousand Talents Program” and “131 Project” of Tianjin City. Y.S. acknowledge the National Supercomputing Center in Shenzhen for providing the computational resources and materials studio (version 7.0).

**Conflicts of Interest:** The authors declare no conflict of interest.

## References

1. Davis, S.J.; Lewis, N.S.; Shaner, M.; Aggarwal, S.; Arent, D.; Azevedo, I.L.; Benson, S.M.; Bradley, T.; Brouwer, J.; Chiang, Y.-M.; et al. Net-zero emissions energy systems. *Science* **2018**, *360*, eaas9793. [CrossRef]
2. The State of Greenhouse Gases in the Atmosphere Based on Global Observations through 2016. Available online: <https://meetingorganizer.copernicus.org/EGU2017/EGU2017-8824-1.pdf> (accessed on 8 May 2019).
3. Sanz-Perez, E.S.; Murdock, C.R.; Didas, S.A.; Jones, C.W. Direct capture of CO<sub>2</sub> from ambient air. *Chem. Rev.* **2016**, *116*, 11840–11876. [CrossRef] [PubMed]
4. Bui, M.; Adjiman, C.S.; Bardow, A.; Anthony, E.J.; Boston, A.; Brown, S.; Fennell, P.S.; Fuss, S.; Galindo, A.; Hackett, L.A.; et al. Carbon capture and storage (CCS): The way forward. *Energy Environ. Sci.* **2018**, *11*, 1062–1176.
5. Olajossy, A. Effective recovery of methane from coal mine methane gas by vacuum pressure swing adsorption: A pilot scale case study. *Chem. Eng. Sci.* **2013**, *1*, 46–54. [CrossRef]
6. Nanda, S.; Reddy, S.N.; Mitra, S.K.; Kozinski, J.A. The progressive routes for carbon capture and sequestration. *Energy Sci. Eng.* **2016**, *4*, 99–122. [CrossRef]
7. Sholl, D.S.; Lively, R.P. Seven chemical separations to change the world. *Nature* **2016**, *532*, 435–437. [CrossRef] [PubMed]
8. Baena-Moreno, F.M.; Rodriguez-Galan, M.; Vega, F.; Alonso-Farinas, B.; Vilches Arenas, L.F.; Navarrete, B. Carbon capture and utilization technologies: A literature review and recent advances. *Energy Sources Part A* **2019**, *41*, 1403–1433. [CrossRef]
9. Wilberforce, T.; Baroutaji, A.; Soudan, B.; Al-Alami, A.H.; Olabi, A.G. Outlook of carbon capture technology and challenges. *Sci. Total Environ.* **2019**, *657*, 56–72. [CrossRef] [PubMed]
10. Li, Y.; Wang, H.P.; Liao, C.-Y.; Zhao, X.; Hsiung, T.-L.; Liu, S.-H.; Chang, S.-G. Dual alkali solvent system for CO<sub>2</sub> capture from flue gas. *Environ. Sci. Technol.* **2017**, *51*, 8824–8831. [CrossRef]
11. Cachaza, A.; Gomez-Diaz, D.; Montans, A.; Navaza, J.M.; Rumbo, A. Carbon dioxide chemical absorption by solvents based on diamine and amines blend. *AIChE J.* **2018**, *64*, 2702–2710. [CrossRef]
12. Yu, J.; Xie, L.-H.; Li, J.-R.; Ma, Y.; Seminario, J.M.; Balbuena, P.B. CO<sub>2</sub> capture and separations using MOFs: Computational and experimental studies. *Chem. Rev.* **2017**, *117*, 9674–9754. [CrossRef] [PubMed]
13. Oschatz, M.; Antonietti, M. A search for selectivity to enable CO<sub>2</sub> capture with porous adsorbents. *Energy Environ. Sci.* **2018**, *11*, 57–70. [CrossRef]
14. Li, J.-R.; Kuppler, R.J.; Zhou, H.-C. Selective gas adsorption and separation in metal-organic frameworks. *Chem. Soc. Rev.* **2009**, *38*, 1477–1504. [CrossRef] [PubMed]
15. Zou, L.; Sun, Y.; Che, S.; Yang, X.; Wang, X.; Bosch, M.; Wang, Q.; Li, H.; Smith, M.; Yuan, S.; et al. Porous organic polymers for post-combustion carbon capture. *Adv. Mater.* **2017**, *29*, 1700229. [CrossRef] [PubMed]
16. Zhu, L.; Zhang, Y.-B. Crystallization of covalent organic frameworks for gas storage applications. *Molecules* **2017**, *22*, 1149. [CrossRef] [PubMed]
17. Li, J.-R.; Ma, Y.; McCarthy, M.C.; Sculley, J.; Yu, J.; Jeong, H.-K.; Balbuena, P.B.; Zhou, H.-C. Carbon dioxide capture-related gas adsorption and separation in metal-organic frameworks. *Coord. Chem. Rev.* **2011**, *255*, 1791–1823. [CrossRef]
18. D’Amato, R.; Donnadio, A.; Carta, M.; Sangregorio, C.; Tiana, D.; Vivani, R.; Taddei, M.; Costantino, F. Water-based synthesis and enhanced CO<sub>2</sub> capture performance of perfluorinated cerium-based metal-organic frameworks with UiO-66 and MIL-140 topology. *ACS Sustainable Chem. Eng.* **2019**, *7*, 394–402. [CrossRef]

19. Wang, Y.; Hu, Z.; Kundu, T.; Cheng, Y.; Dong, J.; Qian, Y.; Zhai, L.; Zhao, D. Metal-organic frameworks with reduced hydrophilicity for postcombustion CO<sub>2</sub> capture from wet flue gas. *ACS Sustainable Chem. Eng.* **2018**, *6*, 11904–11912. [[CrossRef](#)]
20. Cavka, J.H.; Jakobsen, S.; Olsbye, U.; Guillou, N.; Lamberti, C.; Bordiga, S.; Lillerud, K.P. A new zirconium inorganic building brick forming metal organic frameworks with exceptional stability. *J. Am. Chem. Soc.* **2008**, *130*, 13850–13851. [[CrossRef](#)]
21. Peterson, G.W.; Mahle, J.J.; DeCoste, J.B.; Gordon, W.O.; Rossin, J.A. Extraordinary NO<sub>2</sub> removal by the metal-organic framework UiO-66-NH<sub>2</sub>. *Angew. Chem. Int. Ed.* **2016**, *55*, 6235–6238. [[CrossRef](#)] [[PubMed](#)]
22. Rapti, S.; Pournara, A.; Sarma, D.; Papadas, I.T.; Armatas, G.S.; Hassan, Y.S.; Alkordi, M.H.; Kanatzidis, M.G.; Manos, M.J. Rapid, green and inexpensive synthesis of high quality UiO-66 amino-functionalized materials with exceptional capability for removal of hexavalent chromium from industrial waste. *Inorg. Chem. Front.* **2016**, *3*, 635–644. [[CrossRef](#)]
23. Zhan, X.-Q.; Tsai, F.-C.; Xie, L.; Zhang, K.-D.; Liu, H.-L.; Ma, N.; Shi, D.; Jiang, T. Ligands-coordinated Zr-based MOF for wastewater treatment. *Nanomaterials* **2018**, *8*, 655. [[CrossRef](#)]
24. Liu, X.L.; Demir, N.K.; Wu, Z.T.; Li, K. Highly water-stable zirconium metal organic framework UiO-66 membranes supported on alumina hollow fibers for desalination. *J. Am. Chem. Soc.* **2015**, *137*, 6999–7002. [[CrossRef](#)] [[PubMed](#)]
25. Huang, A.; Wan, L.; Caro, J. Microwave-assisted synthesis of well-shaped UiO-66-NH<sub>2</sub> with high CO<sub>2</sub> adsorption capacity. *Mater. Res. Bull.* **2018**, *98*, 308–313. [[CrossRef](#)]
26. Cam Loc, L.; Thi Thuy Van, N.; Tri, N.; Tien Cuong, H. Synthesis, characterization and adsorption ability of UiO-66-NH<sub>2</sub>. *Adv. Nat. Sci. Nanosci. Nanotec.* **2015**, *6*, 2.
27. Cmarik, G.E.; Kim, M.; Cohen, S.M.; Walton, K.S. Tuning the adsorption properties of UiO-66 via ligand functionalization. *Langmuir* **2012**, *28*, 15606–15613. [[CrossRef](#)] [[PubMed](#)]
28. Zhang, X.-F.; Feng, Y.; Wang, Z.; Jia, M.; Yao, J. Fabrication of cellulose nanofibrils/UiO-66-NH<sub>2</sub> composite membrane for CO<sub>2</sub>/N<sub>2</sub> separation. *J. Membrane Sci.* **2018**, *568*, 10–16. [[CrossRef](#)]
29. Nguyen, T.-B.; Rodrigue, D.; Kaliaguine, S. In-situ cross interface linking of PIM-1 polymer and UiO-66-NH<sub>2</sub> for outstanding gas separation and physical aging control. *J. Membrane Sci.* **2018**, *548*, 429–438.
30. Valenzano, L.; Civalleri, B.; Chavan, S.; Bordiga, S.; Nilsen, M.H.; Jakobsen, S.; Lillerud, K.P.; Lamberti, C. Disclosing the complex structure of UiO-66 metal organic framework: A synergic combination of experiment and theory. *Chem. Mater.* **2011**, *23*, 1700–1718. [[CrossRef](#)]
31. DeStefano, M.R.; Islamoglu, T.; Hupp, J.T.; Farha, O.K. Room-temperature synthesis of UiO-66 and thermal modulation of densities of defect sites. *Chem. Mater.* **2017**, *29*, 1357–1361. [[CrossRef](#)]
32. Trickett, C.A.; Gagnon, K.J.; Lee, S.; Gandara, F.; Buergi, H.-B.; Yaghi, O.M. Definitive molecular level characterization of defects in UiO-66 crystals. *Angew. Chem. Int. Ed.* **2015**, *54*, 11162–11167. [[CrossRef](#)]
33. Katz, M.J.; Brown, Z.J.; Colon, Y.J.; Siu, P.W.; Scheidt, K.A.; Snurr, R.Q.; Hupp, J.T.; Farha, O.K. A facile synthesis of UiO-66, UiO-67 and their derivatives. *Chem. Commun.* **2013**, *49*, 9449–9451. [[CrossRef](#)]
34. Li, L.; Yang, J.; Li, J.; Chen, Y.; Li, J. Separation of CO<sub>2</sub>/CH<sub>4</sub> and CH<sub>4</sub>/N<sub>2</sub> mixtures by M/DOBDC: A detailed dynamic comparison with MIL-100(Cr) and activated carbon. *Microporous Mesoporous Mater.* **2014**, *198*, 236–246. [[CrossRef](#)]
35. Ling, Y.; Yang, F.; Deng, M.; Chen, Z.; Liu, X.; Weng, L.; Zhou, Y. Novel iso-reticular Zn(II) metal-organic frameworks constructed by trinuclear-triangular and paddle-wheel units: Synthesis, structure and gas adsorption. *Dalton Trans.* **2012**, *41*, 4007–4011. [[CrossRef](#)]
36. Millward, A.R.; Yaghi, O.M. Metal-organic frameworks with exceptionally high capacity for storage of carbon dioxide at room temperature. *J. Am. Chem. Soc.* **2005**, *127*, 17998–17999. [[CrossRef](#)]
37. Ethiraj, J.; Albanese, E.; Civalleri, B.; Vitillo, J.G.; Bonino, F.; Chavan, S.; Shearer, G.C.; Lillerud, K.P.; Bordiga, S. Carbon dioxide adsorption in amine-functionalized mixed-ligand metal-organic frameworks of UiO-66 topology. *ChemSusChem* **2014**, *7*, 3382–3388. [[CrossRef](#)] [[PubMed](#)]
38. Myers, A.L.; Prausnitz, J.M. Thermodynamics of mixed-gas adsorption. *AIChE J.* **1965**, *11*, 121–127. [[CrossRef](#)]
39. Chen, Y.; Lv, D.; Wu, J.; Xiao, J.; Xi, H.; Xia, Q.; Li, Z. A new MOF-505@GO composite with high selectivity for CO<sub>2</sub>/CH<sub>4</sub> and CO<sub>2</sub>/N<sub>2</sub> separation. *Chem. Eng. J.* **2017**, *308*, 1065–1072. [[CrossRef](#)]
40. Lin, R.B.; Chen, D.; Lin, Y.Y.; Zhang, J.P.; Chen, X.M. A zeolite-like zinc triazolate framework with high gas adsorption and separation performance. *Inorg. Chem.* **2012**, *51*, 9950–9955. [[CrossRef](#)]

41. Lefebvre, C.; Rubez, G.; Khartabil, H.; Boisson, J.-C.; Contreras-García, J.; Hénon, E. Accurately extracting the signature of intermolecular interactions present in the NCI plot of the reduced density gradient versus electron density. *Phys. Chem. Chem. Phys.* **2017**, *19*, 17928–17936. [[CrossRef](#)]
42. Yao, K.X.; Chen, Y.; Lu, Y.; Zhao, Y.; Ding, Y. Ultramicroporous carbon with extremely narrow pore distribution and very high nitrogen doping for efficient methane mixture gases upgrading. *Carbon* **2017**, *122*, 258–265. [[CrossRef](#)]
43. Lu, Y.; He, J.; Chen, Y.; Wang, H.; Zhao, Y.; Han, Y.; Ding, Y. Effective acetylene/ethylene separation at ambient conditions by a pigment-based covalent-triazine framework. *Macromol. Rapid Commun.* **2018**, *39*, 1700468. [[CrossRef](#)] [[PubMed](#)]
44. *Adsorption Locator*; Version 7.0; For A Module in the Materials Studio Modeling Software Package; Accelrys Inc.: San Diego, CA, USA.
45. Perdew, J.P.; Burke, K.; Ernzerhof, M. Generalized gradient approximation made simple. *Phys. Rev. Lett.* **1996**, *77*, 3865–3868. [[CrossRef](#)]
46. Delley, B. An all-electron numerical method for solving the local density functional for polyatomic molecules. *J. Chem. Phys.* **1990**, *92*, 508–517. [[CrossRef](#)]
47. Delley, B. From molecules to solids with the DMol3 approach. *J. Chem. Phys.* **2000**, *113*, 7756–7764. [[CrossRef](#)]
48. Lu, T.; Chen, F. Multiwfn: A multifunctional wavefunction analyzer. *J. Comput. Chem.* **2012**, *33*, 580–592. [[CrossRef](#)] [[PubMed](#)]

**Sample Availability:** Samples of the compounds are available from the authors.



© 2019 by the authors. Licensee MDPI, Basel, Switzerland. This article is an open access article distributed under the terms and conditions of the Creative Commons Attribution (CC BY) license (<http://creativecommons.org/licenses/by/4.0/>).